Raman-like resonant secondary emission causes valley coherence in CVD-grown monolayer MoS_2

Naotaka Yoshikawa,[1,2,*] Shuntaro Tani,[2] and Koichiro Tanaka[1,2,†]

[1]*Department of Physics, Graduate School of Science, Kyoto University, Sakyo-ku, Kyoto 606-8502, Japan*

[2]*Institute for Integrated Cell-Material Sciences (WPI-iCeMS), Kyoto University, Sakyo-ku, Kyoto 606-8501, Japan*

(Received 17 June 2016; revised manuscript received 19 January 2017; published 16 March 2017)

Monolayer transition metal dichalcogenides are promising materials for "valleytronics." They have band gaps at energy-degenerate K and K' valleys with opposite spins. Due to the lack of inversion symmetry, electron-hole pairs can be selectively created at K or K' valleys by circularly polarized photons. In addition, linearly polarized light excitation creates the coherent superposition of exciton valley states, referred to as the generation of valley coherence. In this study we performed polarization resolved photoluminescence and resonant Raman spectroscopy of CVD-grown monolayer MoS_2. We found that the lowest exciton photoluminescence becomes polarized, indicating the effective generation of valley polarization and valley coherence due to the resonant effect, accompanied by a drastic change of the polarization selection rule of Raman scattering. These results were theoretically explained from the viewpoint of the selection rules of resonant Raman scattering. We conclude that the Raman-like resonant second-order optical process should be the main mechanism of valley coherence.

DOI: 10.1103/PhysRevB.95.115419

Layered transition metal dichalcogenides (TMDs) such as MoS_2, WS_2, $MoSe_2$, and WSe_2 show interesting properties in their monolayer form, including enhanced photoluminescence caused by indirect-to-direct band gap transition [1–4], extremely large exciton and trion binding energy due to the enhancement of Coulomb interaction in the ideal two-dimensional system [5–13], and valley physics arising from inversion symmetry breaking [14–27]. Monolayer TMDs have direct optical band gap at energy degenerate K and K' points of the hexagonal Brillouin zone, and the valley pseudospin is coupled to the real electron spin [14]. The electrons in the K or K' valley can be selectively excited using circularly polarized light due to optical selection rules. Robust valley polarization has been confirmed by the observation of circularly polarized photoluminescence, which exhibits the same helicity as the excitation laser in monolayer TMDs [16–20]. Recently, besides circularly polarized photoluminescence, linearly polarized photoluminescence whose orientation coincides with that of the linearly polarized excitation from neutral excitons was observed in monolayer WSe_2 [21,22]. This result indicates that excitons in different valleys may maintain their phase coherence in the recombination process because excitation with a linearly polarized photon generates a coherent superposition of the exciton states in K and K' valleys. The optical generation and readout of valley coherence are attracting much attention for quantum information applications using a valley index. It is surprising that even with the optical excitation over 100 meV above the exciton 1s state, valley coherence was maintained [21,22]. In general, excitonic coherence is lost during energy relaxation involving scattering processes, causing the depolarization of the exciton photoluminescence. The authors of Ref. [21] claimed that the formation mechanism of the superposition state of excitons in K and K' valleys should include the phonon scattering process to the bottom of valleys and their relative phase remain unchanged due to the symmetric nature of the phonon scattering process within the valley. However, there still remains an unsolved question on the overall optical process of the valley coherence that only the coherence between excitons in the K and K' valley is maintained or both of the coherence between excitons in K and K' valleys and the coherence between exciton states and ground state are maintained in the recombination process.

In this study we have investigated the polarization dependence of the emitted intensity of the exciton photoluminescence and Raman scattering of monolayer MoS_2 grown by chemical vapor deposition (CVD), with circular and linear polarization and at a resonant and nonresonant excitation condition. With resonant excitation, the polarization selection rule of the Raman scattering by the E' phonon is drastically changed, and the exciton photoluminescence simultaneously becomes polarized strongly to have the valley coherence. In principle, the photoluminescence and Raman scattering is indistinguishable at the resonant excitation condition and both of them should be considered as the resonant second-order optical process [28,29]. We theoretically examined the polarization dependence of the photoluminescence and Raman scattering from the viewpoint of the selection rules of resonant Raman scattering by symmetry analysis. As a result, observed polarization memory and simultaneous change of the selection rule strongly suggests that Raman-like resonant secondary emission governs the optical processes and also plays as the main mechanism of valley polarization and valley coherence.

Figure 1(a) shows the photoluminescence excitation (PLE) spectrum of monolayer MoS_2 at 34 K, where the detection energy is set to the emission energy of the bound exciton [30]. The A and B exciton peaks are observed. Figure 1(b) shows the photoluminescence spectrum with 2.33 eV excitation. From the fitting of four Gaussian distributions, the peak energies of the A exciton, trion, B exciton, and bound exciton are estimated to be 1.946, 1.918, 2.11, and 1.71 eV, respectively. The weak, sharp peak at 2.28 eV is assigned to the Raman scattering by the A_1' phonon. Figures 1(c) and 1(d) show the circular and linear polarization-resolved emission spectra with 1.96 eV excitation [red arrow in Fig. 1(a)], which is resonant with the A exciton. One can clearly see that the low energy tail of the A exciton photoluminescence is strongly enhanced due to the resonant

*y.naotaka@scphys.kyoto-u.ac.jp

†kochan@scphys.kyoto-u.ac.jp

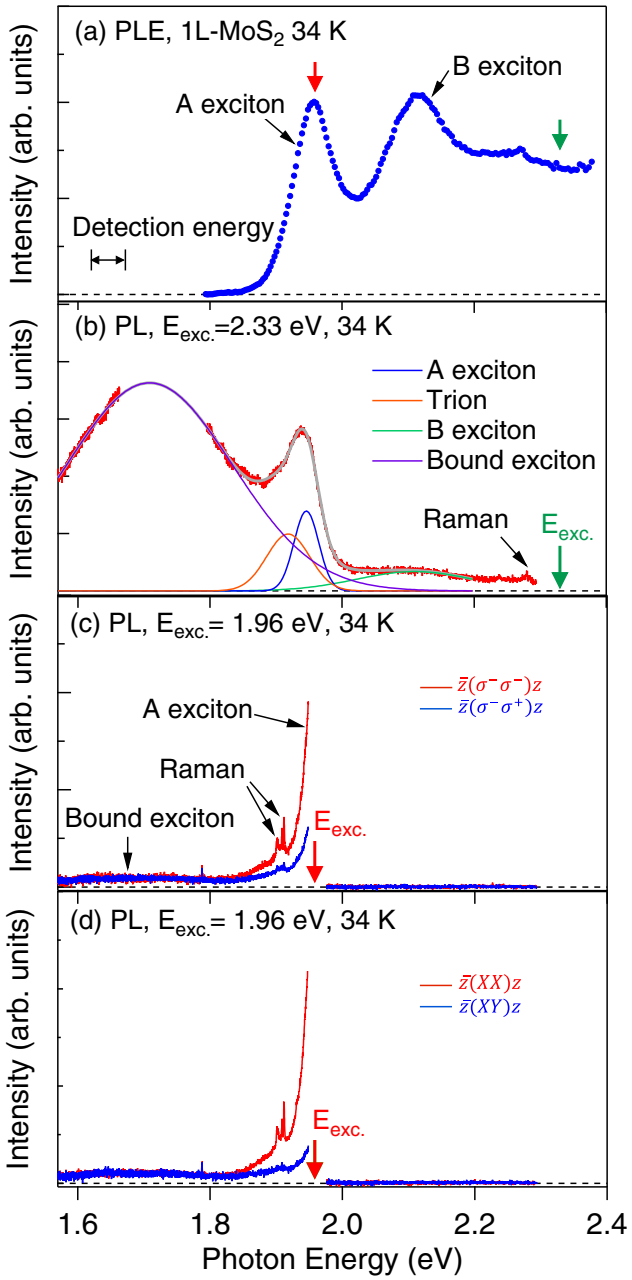

FIG. 1. (a) Photoluminescence excitation (PLE) spectrum of monolayer MoS_2 (1L-MoS_2) at 34 K. Detection energy is set to 1.62–1.67 eV (black arrow). Red and green arrows represent the excitation energies used in this study. (b) Polarization-unresolved photoluminescence spectrum with 2.33 eV excitation (green arrow). Data around 1.7 eV are not shown because there are strong components derived from sapphire substrate in this energy region. Four Gaussian distributions by fitting and the sum of them (gray curve) are also shown. (c) Circular and (d) linear polarization-resolved photoluminescence spectra of monolayer MoS_2 with 1.96 eV excitation (red arrow). Red curve shows co-circular (co-linear) component and blue curve shows anticircular (cross-linear) component. Polarization configurations are represented in accordance with Porto notation.

effect as well as Raman peaks: The emission intensity at the detection energy of 1.94 with 1.96 eV excitation is 12 times as strong as that with the same number of incident photons of 2.33 eV excitation while the intensity of the bound exciton emission is almost unchanged. The low energy tail does not stem from scattered laser light because it was not observed in the spectrum of monolayer MoS_2 at room temperature and in the spectrum of substrate (data not shown). Three sharp peaks around 1.91 eV are assigned to the Raman scattering by E', A_1', and $2LA(M)$ modes. [The detailed Raman spectra are shown in Figs. 3(a) and 3(b).] With circularly (linearly) polarized excitation, the co-circular (co-linear) component of the A exciton photoluminescence is significantly stronger than the anticircular (cross-linear) component, indicating the effective generation and readout of valley polarization (valley coherence). The degrees of polarization are defined as $\rho = [I(\sigma^-) - I(\sigma^+)]/[I(\sigma^-) - I(\sigma^+)]$ for circular polarization and $\rho = [I(X) - I(Y)]/[I(X) - I(Y)]$ for linear polarization. The degree of circular (linear) polarization of the A exciton and trion are estimated to be 0.56 (0.76) and 0.28 (0.43), respectively [30].

Figure 2(a) shows the temperature dependence of the A exciton photoluminescence spectra with 1.96 eV excitation. Here we plot only the component relevant to the A exciton and Raman scattering by subtracting the trion and bound exciton components from the total emission spectra. The higher energy components increase while the lower energy components decrease with higher temperature. This temperature dependence can be understood by considering the A exciton photoluminescence under resonant excitation as the photon emission process through phonon emission or absorption [39]. Figure 2(b) shows the Arrhenius plot of the intensity ratio between anti-Stokes (phonon absorption process) and Stokes (phonon emission process) components for the shift energy of 150 and 200 cm^{-1}. This clearly shows the temperature dependence described by $\frac{I_{\text{anti-Stokes}}}{I_{\text{Stokes}}} = A_0 \exp(-\frac{E_{\text{shift}}}{k_B T})$, which is expected when the photoluminescence is accompanied by phonon emission or absorption. The Stokes components multiplied by $A_0 \exp(-\frac{E_{\text{shift}}}{k_B T})$ versus the inverse of the energy shift are represented by solid curves and the anti-Stokes components by dots in Fig. 2(c). The coincidences of these two spectra mean that the photoluminescence intensity is in accordance with the above equation. The photoluminescence is observed with various and continuous energy shifts, and even with a smaller energy shift than that of the optical phonons ($E_{\text{optical}} > 250\,cm^{-1}$) in monolayer MoS_2. This indicates that the concerned phonons with photoluminescence are not specific ones but combinations of phonons, for example, a combination of two acoustic phonons with finite wave vectors $\boldsymbol{k}$ and $-\boldsymbol{k}$. The related phonons can have various wave vector but the combinations of them should have zero net wave vector in order to satisfy the momentum conservation condition. E_{shift} in the above equation means the total energy of related phonons.

As discussed in detail in previous papers [28,29], photoluminescence and Raman scattering cannot be distinguished in principle when the incident or emitted photon is resonant to the exciton. The photoluminescence and Raman scattering should be uniformly understood in the framework of the resonant second-order optical process with phonon emission or absorption. Therefore, the exciton photoluminescence under resonant excitation and the resonant Raman scattering by E', A_1', and $2LA(M)$ observed in Figs. 1(c) and 1(d) may be governed by the same mechanism apart from the number

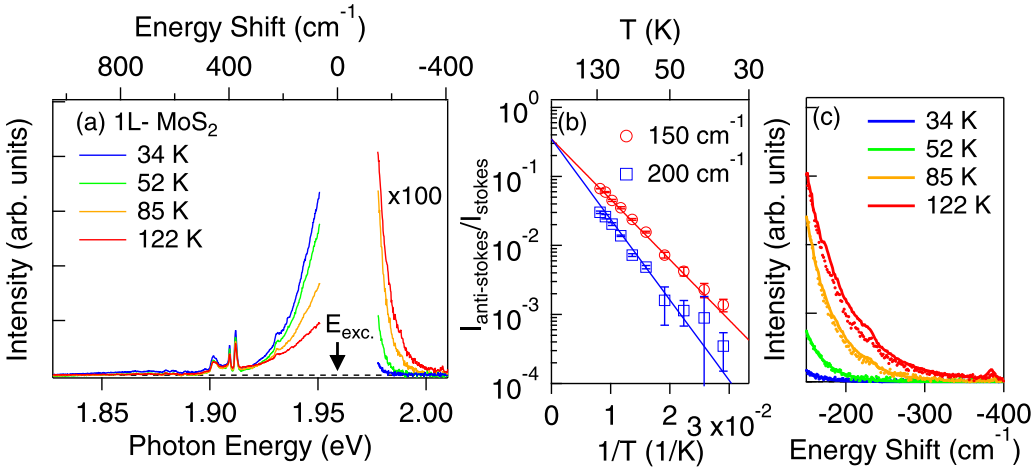

FIG. 2. (a) Emission spectra of the A exciton and Raman scattering with various temperatures with 1.96 eV excitation (indicated by black arrow). Higher energy (anti-Stokes) components are multiplied by a hundred for clarity. (b) Arrhenius plot of intensity ratio between anti-Stokes and Stokes components for 150 and 200 cm^{-1} energy shift. Solid lines are eye guides. (c) Stokes components multiplied by $A_0\exp(-E_{\text{shift}}/k_BT)$ (solid curves) versus inverse of energy shift and anti-Stokes components (dotted curves).

or mode of concerned phonons. Figures 3(a) and 3(b) show the circular and linear polarization-resolved Raman spectra with 1.96 eV excitation at 34 K, which are the enlarged view of Figs. 1(c) and 1(d). With circularly (linearly) polarized excitation, the co-circular (co-linear) components of three Raman peaks are stronger than the anticircular (cross-linear) components. In Figs. 3(c) and 3(d) the normalized intensities of the three Raman peaks are plotted in the polar coordinate as a function of the detected polarization angle for the given incident laser polarization marked by black arrows. These polar plots show cosine dependence on the detection angle, indicating that the scattered photon has the same helicity of circular polarization [Fig. 3(c)] and the same direction of linear polarization [Fig. 3(d)] as the excitation photon. The detection angle dependence of the A exciton photoluminescence [1.940–1.948 eV in Figs. 1(c) and 1(d)] are also shown in Figs. 3(e) and 3(f). These polarization features are none other than the valley polarization and coherence. The coincidence of the detection polarization dependence of the A exciton photoluminescence and Raman scattering indicates that the A exciton photoluminescence is polarized just as the resonant Raman scattering is. Thus, all of the optical processes consisting of Raman scattering and photoluminescence should be considered as different pathways in the same resonant second-order optical process through phonon emission or absorption. The mechanism we propose here is consistent with that in Ref. [21], but we believe that our model gives a more detailed illustration of the valley coherence. Our observation of the polarization memory in resonant Raman lines and its coincidence of the polarization properties with the photoluminescence strongly indicate that the mechanism of valley coherence should be considered as Raman-like secondary emission, where the coherence between exciton states and ground state in addition to the coherence between excitons in K and K' valleys is maintained in the recombination process.

Figures 3(g) and 3(h) show the polarization-resolved nonresonant Raman spectra with 2.33 eV excitation at room temperature. The detection polarization dependence of the E' peak is clearly different from that with resonant excitation. The polar plots shown in Figs. 3(i) and 3(j) confirm that the Raman scattered photon by E' shows completely opposite helicity to the incident photon with circular polarization excitation and constant intensity for all directions of detection polarization with linear polarization excitation. The polarization selection rules with Raman tensor analysis well reproduce the observed detection polarization dependencies for nonresonant Raman scattering [40,41]. We can also recognize a small peak indicated by allows in Figs. 3(g) and 3(h) whose shift energy is slightly lower than the E' mode. The polarization dependence shows that this peak is a breathing mode, that is, the only co-circular (co-linear) component appears. In addition, the detection angle dependence of the A exciton photoluminescence with the same excitation condition shown in Figs. 3(k) and 3(l) confirm that the A exciton photoluminescence is completely depolarized.

By comparing results with resonant and nonresonant excitation conditions, valley polarization and coherence of photoluminescence clearly observed in the resonant condition [Figs. 3(e) and 3(f)] completely disappear in the nonresonant condition synchronously with the recovery of the polarization selection rule of the Raman scattering. Figure 4 shows the schematics of photoluminescence and Raman scattering. With the nonresonant excitation, ordinary luminescence under the energy relaxation [Fig. 4(a)] is clearly distinguishable from nonresonant Raman scattering [Fig. 4(b)] in the spectral peak position. With the resonant excitation, the exciton with the phonon is generated. The luminescence following the emission of the phonon [Fig. 4(c)] and Raman scattering by the same phonon [Fig. 4(d)] are indistinguishable. These resonant secondary emissions are featured by luminescence-like and Raman-like components by investigating time profiles with various excitation energies [42], dephasing time of the excited state [43], and polarization of the emitted photon [44]. The luminescence-like component has no phase and polarization memories in general. We expect that the main contribution of the A exciton photoluminescence with resonant excitation is the Raman-like component in the resonant second-order

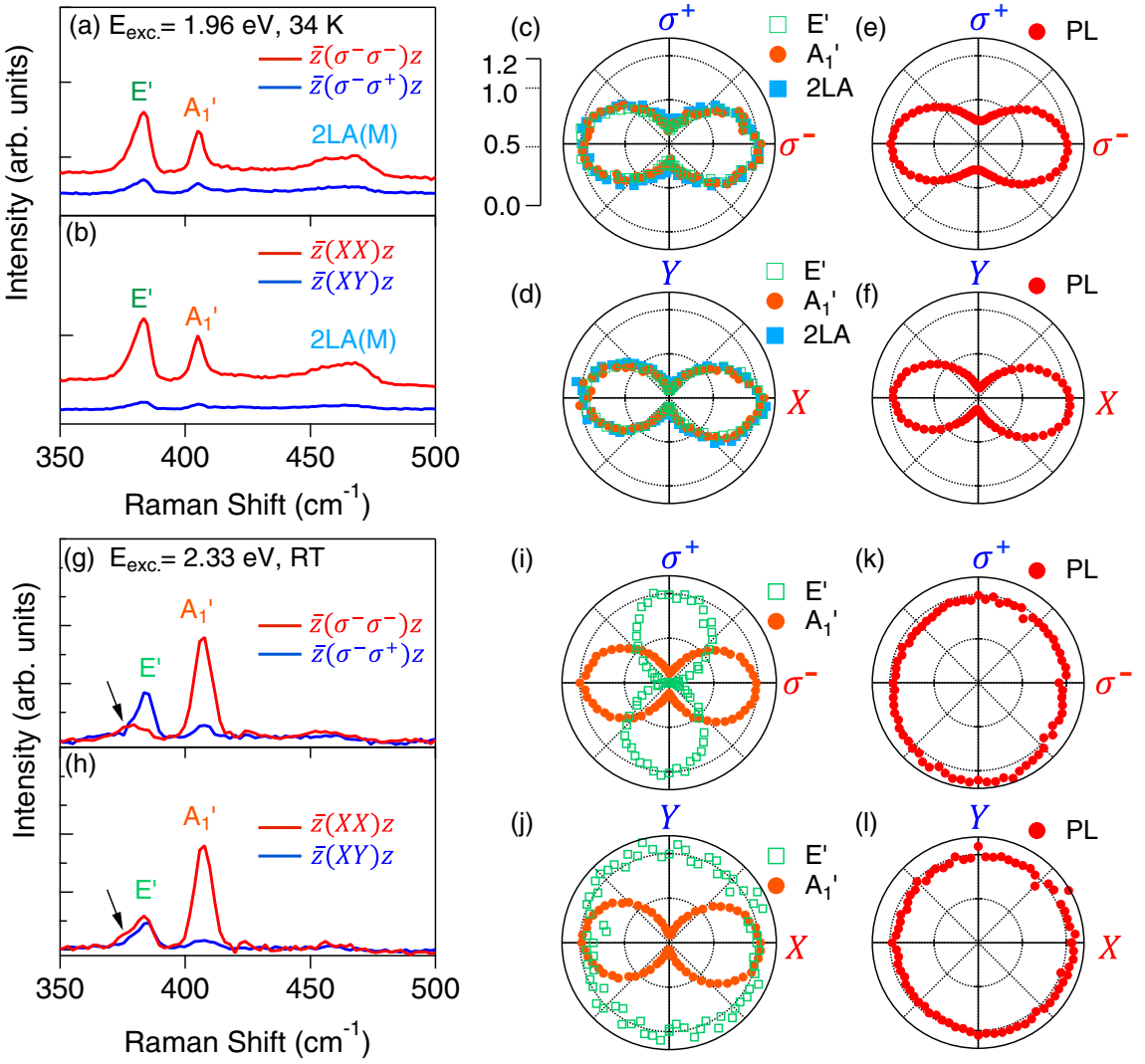

FIG. 3. Polarization-resolved (a) and (b) resonant and (g) and (h) nonresonant Raman scattering spectra of monolayer MoS_2. Incident laser is (a) circularly polarized, 1.96 eV, (b) linearly polarized, 1.96 eV, (g) circularly polarized, 2.33 eV, and (h) linearly polarized, 2.33 eV. Red curve shows co-circular (co-linear) component and blue curve shows anticircular (cross-linear) component. Normalized intensity of (c), (d), (i), and (j) Raman scattering and (e), (f), (k), and (l) A exciton photoluminescence (PL) as a function of detection angle.

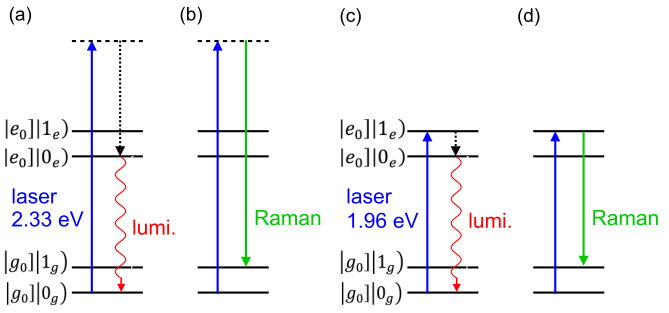

FIG. 4. Schematics of A exciton photoluminescence and Raman scattering with (a) and (b) nonresonant excitation and (c) and (d) resonant excitation. Solid and dashed lines represent real exciton states and virtual intermediate states, respectively. Dotted arrows indicate the energy relaxation involving scattering processes causing decoherence.

optical process because its polarization memory is clearly conserved. Therefore, we theoretically examine the polarization of the photoluminescence and Raman scattering under resonant excitation from the viewpoint of the selection rules of resonant Raman scattering.

In the case of nonresonant Raman scattering, Raman tensors are given by the Kramers-Heisenberg-Dirac dispersion formula [45,46], and the polarization selection rules are consistent with the experimental results [Figs. 3(g)–3(j)] [40,41]. In the resonant case, also starting from the Kramers-Heisenberg-Dirac dispersion formula, the Raman tensor α of Stokes Raman scattering with N-phonon emission is given by (Albrecht's A term) [47]

$$(\alpha_{\rho\sigma})_{g0gN} = \sum_{v} \frac{[g^0|D_\rho|e^0][e^0|D_\sigma|g^0]}{E_{ev} - E_{g0} - E_i - i\Gamma_{ev}} (0_g|v_e)(v_e|N_g), \tag{1}$$

E_{g0} and E_{ev} denote the energy of the $|g]|0_g)$ and $|e]|v_e)$ states under adiabatic approximations. $|\ g]$ and $|\ e]$ are the electronic ground state and excited state, and $|\ g^0]$ and $|\ e^0]$ are those for the equilibrium lattice configuration with the electronic ground state. $|v_g)$ and $|v_e)$ represent v-phonon states on the ground and excited adiabatic potential surfaces, respectively. E_i is the energy of the incident photon. Γ_{ev} is the damping constant for the $|e]|v_e)$ state. D_σ and D_ρ are the σ and ρ components of the electric dipole moment operator. The symmetry of the electron and hole at the K and K' points including the real spin is described by the C_{3h} double point group symmetry. The irreducible representations of the optically active exciton $1s$ states in the K and K' valleys are Γ_3 and Γ_2, which is the same symmetry as σ^- and σ^+ photons, respectively [48]. The symmetry analysis well describes the spin and valley properties including the optical selection rules in monolayer TMDs, confirming that the resonant Raman scattering is directly related to the valley physics. By evaluating the matrix element $[g^0|D_\rho|e^0][e^0|D_\sigma|g^0]$, it is evident that the intensity of Raman scattering with resonant excitation is nonzero only when the polarization of the scattered photon is the same as the incident photon. This prediction clearly explains the experimental facts that both the resonant Raman scattering and photoluminescence have the same polarization as the incident photon, i.e., the valley polarization and coherence. Details of the theoretical approach are shown in the Supplemental Material [30].

The polarization dependence of the A exciton photoluminescence and resonant Raman scattering by E', $A_1{}'$, and $2LA(M)$ phonons indicate that the second-order optical process should be dominated by the Raman-like component. To further check this point, we measured the time response of the photoluminescence. Photoluminescence decays as fast as the time resolution of our time-resolved experimental setup, indicating that the lifetime is faster than 10 ps. Several groups also reported such a fast lifetime of the exciton in monolayer TMDs [49–54]. The origin of the short lifetime has been attributed to the nonradiative process in the excited state. This lifetime is in the same order as the decoherence time [27,53,54]. Due to this short exciton lifetime (fast nonradiative decay), the intensity of the Raman-like component may become dominant in the time-integrated secondary emission spectrum even under the resonant condition. Therefore, the valley polarization can also be achieved mainly by the Raman-like resonant secondary emission in the sample with a short lifetime. If the exciton lifetime was much longer, valley polarization could be realized even by ordinary luminescence, since valley polarization can be maintained through intravalley energy relaxation processes. In such a case, it is expected that valley polarization and coherence show different behavior in time domain.

In summary, we investigated the polarization dependence of the emitted intensity of Raman scattering and the exciton photoluminescence of CVD-grown monolayer MoS_2, with circular and linear polarization at a resonant and a nonresonant excitation condition. We found that the polarization selection rule of the Raman scattering by the E' phonon is drastically changed, and the exciton photoluminescence becomes strongly polarized with resonant excitation. These results are uniformly understood from the viewpoint of the selection rules of Raman scattering, which is theoretically examined by the symmetry analysis using group theory. We conclude that the main mechanism of valley polarization and valley coherence should be domination of the Raman-like component in the resonant second-order optical process. Time resolved spectroscopy with a higher time resolution or the use of a sample with a longer lifetime, for example, a superacid treated one [55,56], will promote further understanding.

This work was supported by a Grant-in-Aid for Scientific Research (A) (Grant No. 26247052). N.Y. was supported by a JSPS fellowship (Grant No. 16J10537).

[1] A. Splendiani, L. Sun, Y. Zhang, T. Li, J. Kim, C. -Y. Chim, G. Galli, and F. Wang, Nano Lett. **10**, 1271 (2010).
[2] K. F. Mak, C. Lee, J. Hone, J. Shan, and T. F. Heinz, Phys. Rev. Lett. **105**, 136805 (2010).
[3] Y. Zhang, T. -R. Chang, B. Zhou, Y. -T. Cui, H. Yan, Z. Liu, F. Schmitt, J. Lee, R. Moore, Y. Chen, H. Lin, H.-T. Jeng, S.-K. Mo, Z. Hussain, A. Bansil, and Z.-X. Shen, Nat. Nanotechnol. **9**, 111 (2013).
[4] W. Zhao, Z. Ghorannevis, L. Chu, M. Toh, C. Kloc, P.-H. Tan, and G. Eda, ACS Nano **7**, 791 (2013).
[5] K. F. Mak, K. He, C. Lee, G. H. Lee, J. Hone, T. F. Heinz, and J. Shan, Nat. Mat. **12**, 207 (2013).
[6] A. Chernikov, T. C. Berkelbach, H. M. Hill, A. Rigosi, Y. Li, O. B. Aslan, D. R. Reichman, M. S. Hybertsen, and T. F. Heinz, Phys. Rev. Lett. **113**, 076802 (2014).
[7] G. Wang, X. Marie, I. Gerber, T. Amand, D. Lagarde, L. Bouet, M. Vidal, A. Balocchi, and B. Urbaszek, Phys. Rev. Lett. **114**, 097403 (2015).
[8] D. Y. Qiu, F. H. da Jornada, and S. G. Louie, Phys. Rev. Lett. **111**, 216805 (2013).
[9] Z. Ye, T. Cao, K. O'Brien, H. Zhu, X. Yin, Y. Wang, S. G. Louie, and X. Zhang, Nature (London) **513**, 214 (2014).
[10] C. Zhang, A. Johnson, C.-L. Hsu, L.-J. Li, and C.-K. Shih, Nano Lett. **14**, 2443 (2014).
[11] K. He, N. Kumar, L. Zhao, Z. Wang, K. F. Mak, H. Zhao, and J. Shan, Phys. Rev. Lett. **113**, 026803 (2014).
[12] M. M. Ugeda, A. J. Bradley, S.-F. Shi, F. H. da Jornada, Y. Zhang, D. Y. Qiu, W. Ruan, S.-K. Mo, Z. Hussain, Z.-X. Shen, F. Wang, S. G. Louie, and M. F. Crommie, Nat. Mater. **13**, 1091 (2014).
[13] S. Cha, J. H. Sung, S. Sim, J. Park, H. Heo, M.-H. Jo, and H. Choi, Nat. Commun. **7**, 10768 (2016).
[14] D. Xiao, G.-B. Liu, W. Feng, X. Xu, and W. Yao, Phys. Rev. Lett. **108**, 196802 (2012).
[15] X. Xu, W. Yao, D. Xiao, and T. F. Heinz, Nat. Phys. **10**, 343 (2014).
[16] K. F. Mak, K. He, J. Shan, and T. F. Heinz, Nat. Nanotechnol. **7**, 494 (2012).
[17] H. Zeng, J. Dai, W. Yao, D. Xiao, and X. Cui, X. Nat. Nanotechnol. **7**, 490 (2012).

[18] T. Cao, G. Wang, W. Han, H. Ye, C. Zhu, J. Shi, Q. Niu, P. Tan, E. Wang, B. Liu, and J. Feng, Nat. Commun. **3**, 887 (2012).
[19] G. Kioseoglou, A. T. Hanbicki, M. Currie, A. L. Friedman, D. Gunlycke, and B. T. Jonker, Appl. Phys. Lett. **101**, 221907 (2012).
[20] G. Sallen, L. Bouet, X. Marie, G. Wang, C. R. Zhu, W. P. Han, Y. Lu, P. H. Tan, T. Amand, B. L. Liu, and B. Urbaszek, Phys. Rev. B **86**, 081301 (2012).
[21] A. M. Jones, H. Yu, N. J. Ghimire, S. Wu, G. Aivazian, J. S. Ross, B. Zhao, J. Yan, D. G. Mandrus, D. Xiao, W. Yao, and X. Xu, Nat. Nanotechnol. **8**, 634 (2013).
[22] G. Wang, M. M. Glazov, C. Robert, T. Amand, X. Marie, and B. Urbaszek, Phys. Rev. Lett. **115**, 117401 (2015).
[23] K. F. Mak, K. L. McGill, J. Park, and P. L. McEuen, Science **344**, 1489 (2014).
[24] J. Kim, X. Hong, C. Jin, S.-F. Shi, C.-Y. Chang, M.-H. Chiu, L.-J. Li, and F. Wang, Science **346**, 1205 (2014).
[25] E. J. Sie, J. W. McIver, Y.-H. Lee, L. Fu, J. Kong, and N. Gedik, Nat. Mater. **14**, 290 (2014).
[26] A. M. Jones, H. Yu, J. R. Schaibley, J. Yan, D. G. Mandrus, T. Taniguchi, K. Watanabe, H. Dery, W. Yao, and X. Xu, Nat. Phys. **12**, 323 (2015).
[27] K. Hao, G. Moody, F. Wu, C. K. Dass, L. Xu, C.-H. Chen, L. Sun, M.-J. Li, A. H. MacDonald, and X. Li, Nat. Phys. **12**, 677 (2016).
[28] Y. Toyozawa, A. Kotani, and A. Sumi, J. Phys. Soc. Jpn. **42**, 1495 (1977).
[29] A. Kotani and Y. Toyozawa, J. Phys. Soc. Jpn. **41**, 1699 (1976).
[30] See Supplemental Material at http://link.aps.org/supplemental/10.1103/PhysRevB.95.115419 which includes Refs. [31–38] for additional details of the experimental methods, the experimental data, data analysis, and theory.
[31] Y. You, X.-X. Zhang, T. C. Berkelbach, M. S. Hybertsen, D. R. Reichman, and T. F. Heinz, Nat. Phys. **11**, 477 (2015).
[32] M. C. Klein, F. Hache, D. Ricard, and C. Flytzanis, Phys. Rev. B **42**, 11123 (1990).
[33] G. Scamarcio, V. Spagnolo, G. Ventruti, M. Lugara, and G. C. Righini, Phys. Rev. B **53**, R10489 (1996).
[34] A. V. Baranov, S. Yamauchi, and Y. Masumoto, Phys. Rev. B **56**, 10332 (1997).
[35] K. Inoue, A. Yamanaka, K. Toba, A. V. Baranov, A. A. Onushchenko, and A. V. Fedorov, Phys. Rev. B **54**, R8321 (1996).
[36] T. D. Krauss and F. W. Wise, Phys. Rev. B **55**, 9860 (1997).
[37] S.-L. Li, H. Miyazaki, H. Song, H. Kuramochi, S. Nakaharai, and K. Tsukagoshi, ACS Nano **6**, 7381 (2012).
[38] B. R. Carvalho, L. M. Malard, J. M. Alves, C. Fantini, and M. A. Pimenta, Phys. Rev. Lett. **114**, 136403 (2015).
[39] J.-U. Lee, J. Park, Y.-W. Son, and H. Cheong, Nanoscale **7**, 3229 (2015).
[40] S.-Y. Chen, C. Zheng, M. S. Fuhrer, and J. Yan, Nano Lett. **15**, 2526 (2015).
[41] Y. Zhao, X. Luo, H. Li, J. Zhang, P. T. Araujo, C. K. Gan, J. Wu, H. Zhang, S. Y. Quek, M. S. Dresselhaus, and Q. Xiong, Nano Lett. **13**, 1007 (2013).
[42] A. Nakamura, M. Shimura, M. Hirai, M. Aihara, and S. Nakashima, Phys. Rev. B **35**, 1281 (1987).
[43] R. P. Stanley, J. Hegarty, R. Fischer, J. Feldmann, E. O. Gobel, R. D. Feldman, and R. F. Austin, Phys. Rev. Lett. **67**, 128 (1991).
[44] N. Pelekanos, J. Ding, Q. Fu, A. V. Nurmikko, S. M. Durbin, M. Kobayashi, and R. L. Gunshor, Phys. Rev. B **43**, 9354 (1991).
[45] H. A. Kramers and W. Heisenberg, Z. Phys. **31**, 681 (1925).
[46] P. A. M. Dirac, Proc. R. Soc. London **A114**, 243 (1927).
[47] A. C. Albrecht, J. Chem. Phys. **34**, 1476 (1961).
[48] M. M. Glazov, T. Amand, X. Marie, D. Lagarde, L. Bouet, and B. Urbaszek, Phys. Rev. B **89**, 201302 (2014).
[49] T. Korn, S. Heydrich, M. Hirmer, J. Schmutzler, and C. Schuller, Appl. Phys. Lett. **99**, 102109 (2011).
[50] D. Lagarde, L. Bouet, X. Marie, C. R. Zhu, B. L. Liu, T. Amand, P. H. Tan, and B. Urbaszek, Phys. Rev. Lett. **112**, 047401 (2014).
[51] C. J. Docherty, P. Parkinson, H. J. Joyce, M.-H. Chiu, C.-H. Chen, M.-Y. Lee, L.-J. Li, L. M. Herz, and M. B. Johnston, ACS Nano **8**, 11147 (2014).
[52] G. Wang, L. Bouet, D. Lagarde, M. Vidal, A. Balocchi, T. Amand, X. Marie, and B. Urbaszek, Phys. Rev. B **90**, 075413 (2014).
[53] T. Jakubczyk, V. Delmonte, M. Koperski, K. Nogajewski, C. Faugeras, W. Langbein, M. Potemski, and J. Kasprzak, Nano Lett. **16**, 5333 (2016).
[54] G. Moody, C. K. Dass, K. Hao, C.-H. Chen, L.-J. Li, A. Singh, K. Tran, G. Clark, X. Xu, G. Berghauser, E. Malic, A. Knorr, and X. Li, Nat. Commun. **6**, 8315 (2015).
[55] M. Amani, D.-H. Lien, D. Kiriya, J. Xiao, A. Azcatl, J. Noh, S. R. Madhvapathy, R. Addou, S. KC, M. Dubey, K. Cho, R. M. Wallace, S.-C. Lee, J.-H. He, J. W. Ager III, X. Zhang, E. Yablonovitch, and A. Javey, Science **350**, 1065 (2015).
[56] M. Amani, T. Peyman, R. Addou, G. H. Ahn, D. Kiriya, D.-H. Lien, J. W. Ager III, R. M. Wallace, and A. Javey, Nano Lett. **16**, 2786 (2016).